

Velocity Estimation and Adaptive Clutter Filtering for Color Flow Imaging

CH. KARGEL, G. HOEBENREICH, G. PLEVNIK, B. TRUMMER, M.F. INSANA
Department of Biomedical Engineering
University of California Davis, CA, USA
Department of Electrical Measurement and Measurement Signal Processing,
Graz University of Technology, Graz, AUSTRIA

Abstract: Preliminary results are presented for a color-flow imaging system being developed to detect early cancer by imaging tissue elasticity and blood flow simultaneously. The principal challenge is to separate blood velocities from movement of the surrounding tissues even though the corresponding Doppler spectra overlap. This report examines a broad range of digital filter designs using pulse-echo measurements from tissue-like materials. Adaptive eigenfilters are most able to separate the sources of physiological motion. When used with an improved autocorrelation technique (2-D autocorrelator), accurate and precise velocity estimates were obtained for slow pulsatile flow in 3-mm-diameter vessels with a peak velocity of 30 mm/s.

Key-Words: Color-Flow Imaging, Velocity Estimation, Autocorrelator, Clutter Rejection Filtering, Adaptive Digital Filter Design.

1 Introduction

Ultrasonic color-flow imaging (CFI) systems provide valuable diagnostic blood velocity information in real-time, noninvasively, and at a cost much less than competing imaging modalities. Unfortunately, most commercial ultrasound scanners are limited in their ability to enable researchers to experiment with new signal processing strategies. For example, new methods for imaging vascularization and perfusion of metastatic tumors while assessing viscoelastic properties hold promise for improved early detection but can't be carried out on commercial scanners. To facilitate such investigations, we built a laboratory system with ample flexibility and present our findings in this report.

It is well known that neoplasms have increased vascularity to supply fast-growing tissues with nutrients [1]. Concurrently, these tissues are structurally remodelled causing them to stiffen due to hyperplasia, fibrosis [2], and desmoplasia [3]. To measure blood velocity and tissue elasticity simultaneously, we are developing a laboratory ultrasound scanner capable of standard as well as novel procedures for imaging blood flow and strain [4]. In this paper we focus on the signal and image processing necessary for estimating low blood velocities, down to a few mm/s, while maintaining the real-time acquisition aspects of the approach. We are also interested in separating flow and strain information by appropriate application of adaptive filters. The latter goal is essential since signal components that carry strain information produce artifacts in CFI and vice versa. To keep image quality high, the variance of velocity and strain estimates must be kept as low as possible

by optimal suppression of certain signal components depending on whether strain or flow is to be estimated.

This paper is organized as follows: in section 2 the conventional autocorrelator is compared with an improved autocorrelator version. Different clutter filter classes are compared in section 3. Finally, experimental results are shown in section 4.

2 Blood Velocity Estimation

The development and implementation of unbiased, low-variance velocity estimators for real-time CFI, particularly for low flow situations, is a challenging signal processing problem. The goal is to suppress noise and clutter from slow-moving tissues surrounding the flowing blood. Suppression is necessary because tissue echoes are orders of magnitude greater than those from blood at frequencies below 15 MHz. The adverse influence of clutter can be reduced by minimizing the size of the echo sample volume, but even if the entire sample volume is inside a blood vessel, clutter from reverberations and transducer side lobes will affect the signal. In this section, we focus on blood velocity estimation by assuming clutter has been removed from the echo signal before estimation. Section 3 describes adaptive filters for this task. A simplified block diagram of our blood velocity measurement system is shown in Fig. 1. Echo signals are amplified, filtered, and decomposed into baseband in-phase (I) and quadrature-phase (Q) components. The IQ-signal generation, computed in software via quadrature demodulation, yields the complex envelope for estimating phase. Required

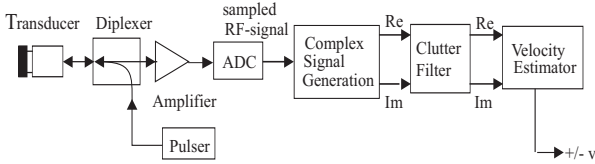


Fig.1: Block diagram of our measurement system for estimating blood velocity

range resolution is achieved in CFI by transmitting ultrasound pulses and range gating the echo signals. Velocity estimators measure the inter-pulse time delay for sequential transmissions at a fixed spatial position. It is assumed that changes in echoes from pulse trains are due to blood movement and noise.

Motion measurements are relative, requiring at least two pulse transmissions at a given line of sight (LOS) before the ultrasound beam can be scanned to the next LOS. For noise reduction, the number of pulse transmissions N , or packet size, is usually greater than 2. Their transmission rate is the pulse repetition frequency f_{PRF} . Recorded radio frequency (RF) echo signals are organized in 2-D arrays where the terms “fast-time” (columns) and “slow-time” (rows) define the direction of the beam axis (RF sampling, index m) and pulse packet dimension (PRF sampling, index n), respectively. The situation is depicted in Fig. 2. Provided that scatterers move with velocity \mathbf{v} , the center Doppler frequency in slow-time direction is $(2v_z \cdot f_0/c)$ where $v_z = v \cdot \cos \Theta$ is the axial velocity component v_z , f_0 is the center frequency of the RF pulse, c is the longitudinal sound speed and Θ is the angle between the beam axis and the velocity vector \mathbf{v} . If echo

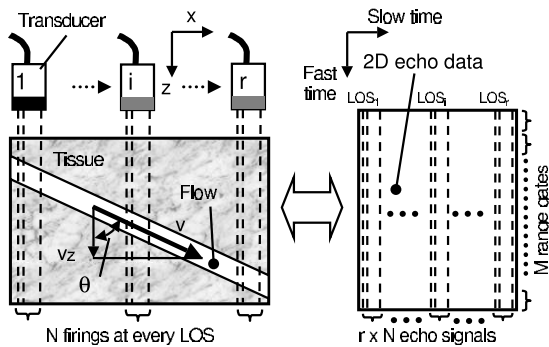


Fig.2: Acquisition in Scan-mode (left) and matrix representation of data (right). Matrix dimensions are $M \times rN$. The situation for M-mode is similar except there is no transducer motion along the x -axis ($r = 1$).

signals originate from a time-steady velocity field, the complex envelope sequence is characterized as a complex Gaussian random process. As such, it is entirely described by its autocorrelation function. Most commercial CFI estimators use a phase domain technique known as the autocorrelator estimator [5] because of its numerical efficiency and real-

time capability. Other velocity estimation techniques are known (e.g., time domain cross-correlation, 2-D Fourier-transform, maximum likelihood estimator, maximum entropy method). While some exhibit superior performance to the autocorrelator, their computational requirements are much greater, thus eliminating real-time applications.

2.1 Conventional (1-D) Autocorrelator

The conventional autocorrelator measures the axial component v_z of the velocity vector by estimating the average phase shift between consecutive echo signals with respect to the central frequency of the transmitted pulses. It can be considered one-dimensional (1-D) as processing occurs along the slow-time axis. The autocorrelator is able to provide estimates of the mean Doppler frequency in the time domain because of a relationship between spectral moments and autocorrelation derivatives. v_z is proportional to the phase of the complex 1-D autocorrelation function $R(\ell)$ at lag $\ell = 1$ in slow-time direction [5]:

$$v_z = \frac{c f_{PRF}}{2 \pi f_0} \arctan \left(\frac{\Im[\hat{R}(1)]}{\Re[\hat{R}(1)]} \right), \quad (1)$$

where \Re and \Im denote the real and imaginary parts. $\hat{R}(\ell)$ is an estimate of the autocorrelation function and can be calculated at each depth m from in-phase $I(n)$ and quadrature-phase $Q(n)$ baseband samples in slow-time direction:

$$\hat{R}(\ell) = \frac{1}{N - \ell} \sum_{n=0}^{N-2} [I(n) + jQ(n)] \cdot [I(n + \ell) - jQ(n + \ell)]. \quad (2)$$

It is known [6] that the autocorrelation frequency estimator yields unbiased estimates in lossless media when the spectrum is symmetric about its mean¹.

2.2 2-D Autocorrelator

The conventional autocorrelator described in section 2.1 is implemented in the vast majority of commercial scanners though it can be improved a great deal without sacrificing the real-time aspect. Under ideal, narrow-band conditions, mean Doppler frequency and thus autocorrelator-based phase estimation provide unbiased velocity estimates. However, the broad-band pulse transmission required in CFI to obtain spatial resolution coupled with the frequency-dependent attenuation in tissues leads to estimation bias. For example, the mean Doppler frequency shift produced by slow physiological blood flow is small

¹Clutter filters, however, may influence the bias and variance of the mean frequency estimates.

when compared with the pulse frequency down-shift caused by tissue attenuation. Also, the stochastic nature of the scattered pressure field produces radio frequency fluctuations while the conventional autocorrelator assumes the RF to be constant. As a result, the uncertainty in mean Doppler frequency measurements increases even for noiseless signals and where flow is constant with time.

The 2-D autocorrelator overcomes these drawbacks with its ability to estimate both the Doppler frequency and radio frequency within each range gate. Furthermore, the RF center frequency of the transducer need not be known or measured beforehand, and therefore spectral changes over time, in temperature, etc. do not influence performance. Another advantage of the 2-D autocorrelator is that explicit estimation of the RF can overcome the bias effect that frequency-dependent attenuation has on the conventional autocorrelator. The 2-D autocorrelator was found to offer a consistently higher velocity precision than the conventional autocorrelator under all conditions [7]. The velocity precision of the 2-D autocorrelator is comparable to the conventional autocorrelator using half the packet size. These facts make the 2-D autocorrelator ideal for estimating low velocities in real-time. v_{z2D} can be estimated using the 2-D autocorrelation function $R_{2D}(k, \ell)$ at lags $(k, \ell) = (0, 1)$ and $(k, \ell) = (1, 0)$ [7]:

$$v_{z2D} = \frac{c}{2} \frac{\frac{f_{PRF}}{2\pi} \arctan\left(\frac{\Im[\hat{R}_{2D}(0,1)]}{\Re[\hat{R}_{2D}(0,1)]}\right)}{f_{dem} + \frac{f_s}{2\pi} \arctan\left(\frac{\Im[\hat{R}_{2D}(1,0)]}{\Re[\hat{R}_{2D}(1,0)]}\right)}. \quad (3)$$

f_{dem} is the demodulation frequency and must be taken into consideration when baseband IQ data are used, f_s is the sampling rate in fast-time direction and \hat{R}_{2D} is the 2-D correlation function estimate of the complex baseband signal $I(m, n) + jQ(m, n)$ given by:

$$\hat{R}_{2D}(k, \ell) = \sum_{m=0}^{M-k-1} \sum_{n=0}^{N-\ell-1} [I(m, n) + jQ(m, n)] \cdot [I(m+k, n+\ell) - jQ(m+k, n+\ell)].$$

The factor $1/[(N-\ell)(M-k)]$ used to obtain unbiased estimates of the correlation function cancels inside the arctan functions.

Fig. 3 shows a comparison of errors obtained from the conventional and 2-D autocorrelators applied to the same IQ data set modelling a constant velocity field. 10000 independent echo signals corresponding to different LOS were used. Each signal was divided into 100 range gates and the packet size was $N = 8$, so error estimates were obtained from $7 \cdot 10^6$ measurements of velocity. This large number is necessary here to derive estimation mean velocities with

adequately low standard deviation. The range gate length was chosen to match the -20 dB transmit pulse duration ($0.512 \mu\text{s}$ or 64 samples at $f_s = 125$ MS/s) with $f_0 = 15$ MHz. Velocity errors are shown for $\text{SNR} = \infty$ and 10 dB. It can be clearly seen that both estimators provide very small absolute errors (bias) while the 2-D autocorrelator additionally provides much lower standard deviations over the entire range of true velocities up to the aliasing velocity. However, the superiority of the 2-D autocorrelator disappears at very low SNR or significant velocity spreads inside the range gates where signals become decorrelated. Velocity spread from turbulent flow is very low in low flow situations. In our experience, SNRs greater than 5 dB are sufficient for superior performance of the 2-D autocorrelator. Depending on measurement parameters (pulse frequency, Doppler shift, pulse and range gate lengths, packet size) SNRs below 0 dB can still provide reliable results.

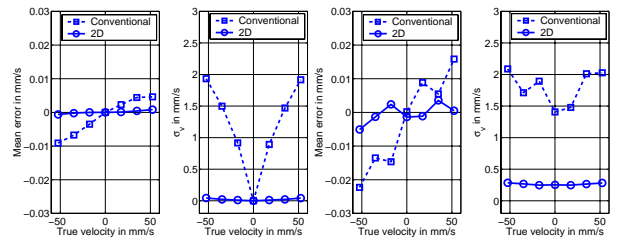


Fig.3: Comparison of conventional and 2-D autocorrelator: mean velocity error (bias) and velocity standard deviation σ_v as a function of velocity for $\text{SNR} = \infty$ (left) and $\text{SNR} = 10$ dB (right). The maximum velocity that can be estimated in this case before aliasing occurs is 73 mm/s.

Applying the 1D autocorrelator or other signal processing methods that estimate only the Doppler shift can increase estimation bias significantly when pulsed ultrasound is used in attenuating media. The results shown in Fig. 4 clearly demonstrate that the 2-D autocorrelator reduces velocity bias in dispersive media with physiological attenuation.

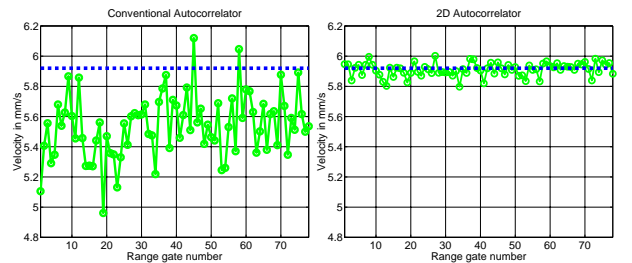


Fig.4: Velocity estimates at $\text{SNR} = 10$ dB. $f_0 = f_{dem} = 15$ MHz, but the center frequency of the echo signals is 14 MHz due to frequency-dependent attenuation. The broken horizontal lines indicate the true velocity of 5.92 mm/s. The 2-D estimator (right side) provides unbiased results with lower σ_v (5.9204 ± 0.029) mm/s, as opposed to the conventional estimator, (5.5327 ± 0.184) mm/s.

3 Clutter-Filter Designs

CFI requires that we choose a packet size (usually $N = 4 \dots 20$) that achieves the best compromise between the need for a high color frame rate and low color noise (velocity errors). Since clutter filters operate along the slow-time axis, only a few echo samples are available for filtering. The design of adaptive high-pass clutter filters for suppressing low-frequency Doppler components in diverse conditions is difficult to optimize. It requires a high stop-band attenuation, flat frequency response in the pass-band and a very small transition region. The demands are greater if velocity estimates are to be combined with strain estimates. We briefly discuss the basic properties of various filter classes before showing experimental results.

3.1 FIR Filters

Given that N is usually small, low-order FIR filters are usually inappropriate because the transition frequency band is too large. Furthermore, the number of valid output samples, N minus the filter order, becomes too small when one considers that the variance for autocorrelation estimates is inversely proportional to the number of valid filter output samples. While we do not consider FIR designs, it has been shown [9] that minimum-phase FIR filters and mirroring techniques can yield acceptable performance.

3.2 Initialized IIR Filters

IIR filters exhibit narrower transition bands than FIR filters for the same order. However, appropriate initialization of the internal filter states must be applied in order to suppress the transient filter response and reduce the “ring-down time”. Three different initialization techniques are investigated in this paper [8, 9]:

- Zero initialization: the initial filter state vector is set to zero for times less than zero. Often, this technique yields unacceptably large transients.
- Step initialization: the filter state vector is set depending on the filter and data values. Transients can be partially suppressed from a priori knowledge that the input signal is dominated by high-amplitude, low Doppler frequency (nearly stationary) clutter. We apply a unit-step input and calculate the internal filter states at $t = \infty$. These values are scaled at each range depth (fast-time) by the amplitude of the first data sample in the pulse packet before being loaded into the filter.
- Projection initialization: the filtered signal is decomposed into steady-state and transient components. Using an appropriate projection oper-

ator [8], which projects the signal in the “transient response subspace”, it is possible to decompose the filtered signal into two orthogonal components and subtract the transient subspace component from the output.

3.3 Regression Filters

Regression filters operate on the assumption that the slowly varying clutter component in the signal can be approximated by a set of curves such as polynomials. The least-square fit to the low-frequency clutter component in the echo signal is subtracted. The curve set is chosen to form an orthonormal basis for a K -dimensional clutter subspace of the N -dimensional signal space. The least-square clutter fit is the projection of the signal into the clutter subspace. The linear filtering operation can be generally expressed in matrix notation:

$$\mathbf{y} = \mathbf{A} \cdot \mathbf{x} \quad (4)$$

with \mathbf{x} being the complex input signal vector, \mathbf{y} being the (filtered) complex output signal vector, both of dimension $N \times 1$, and \mathbf{A} as the filter matrix of dimension $N \times N$:

$$\mathbf{A} = \mathbf{I} - \sum_{k=0}^{K-1} \mathbf{b}_k \cdot \mathbf{b}_k^H, \quad (5)$$

where \mathbf{b}_k is the set of orthonormal basis vectors, often Legendre or Chebychev polynomials, $(\dots)^H$ is the Hermitian operator, and \mathbf{I} is the identity matrix. The frequency response of the filter can be calculated by

$$H(\omega) = 1 - \frac{1}{N} \sum_{k=0}^{K-1} |B_k(\omega)|^2 \quad (6)$$

where $B_k(\omega)$ is the Fourier transform of the basis vector \mathbf{b}_k [10]. In order to design high-pass filters, K must be small. Regression filters are adaptive in the sense that the polynomial coefficients vary depending on the data.

3.4 Adaptive Eigenfilters

The eigenfilter approach is to create basis functions for the clutter space that adapt to specific clutter signal statistics. Since the basis set and coefficients are determined by the data, eigenfilters are truly adaptive. The Hotelling transform² decomposes \mathbf{x} into

²Hotelling was the first to derive the transformation that transforms discrete variables into uncorrelated coefficients. He referred to it as the “method of principal components”. The analogous transformation for transforming continuous data was discovered by Karhunen and Loève.

N orthonormal components by using the eigenvectors ($\mathbf{e}_1, \dots, \mathbf{e}_N$) of the clutter covariance matrix \mathbf{C}_C as basis³:

$$\mathbf{C}_C = \mathcal{E}\{\mathbf{x} \cdot \mathbf{x}^H\} \quad (7)$$

where $\mathcal{E}\{\cdot\}$ is the expected value. Signal components related to large eigenvalues correspond to clutter because clutter signals are usually much larger than flow signals. The Hotelling signal expansion is optimal in the sense that no other transform packs as much energy into the first components (optimum energy concentration property). This means, in our case, that the clutter approximation minimizes the mean square error and therefore a maximum reduction of clutter energy is obtained by removing the component of the signal contained in the subspace spanned by ($\mathbf{e}_1, \dots, \mathbf{e}_K$) with $K < N$. Eqn. 5 and Eqn. 6 can be used to calculate the filter matrix \mathbf{A} and filter frequency response. In a practical situation \mathbf{C}_C is unknown but can be estimated from the data in the region of interest by spatial averaging in fast-time direction:

$$\hat{\mathbf{C}}_C = \frac{1}{m} \sum_{i=1}^m \mathbf{x}_i \cdot \mathbf{x}_i^H \quad (8)$$

Stationarity is not assumed in the estimation of the correlation matrix, and therefore the Eigenvector-based filter is able to adapt even to clutter echos which originate from accelerated tissue.

3.5 Comparison of the Filter Frequency Responses

Fig. 5 shows the frequency responses of the different filter classes described in this paper for a packet size $N=16$. Initialization of second order IIR filters with high-pass butterworth characteristics largely suppresses transients and thereby improves the frequency response towards the steady state case. We would like to remind the reader that, due to the low number of filter input samples, the steady state frequency response can never be achieved. Zero-initialized IIR filters provide a DC attenuation of only about 10 dB which renders CFI in the presence of clutter impossible. Projection-initialized IIR filters and regression filters have very similar frequency responses. The Eigenvector-based high-pass filter has even steeper roll-off than the IIR filter in its steady state.

4 Experimental Results

To study the performance of the 2-D autocorrelator and various clutter filters we conducted the following

³Clutter signals stem from a zero mean complex Gaussian process and hence covariance and correlation matrices are identical.

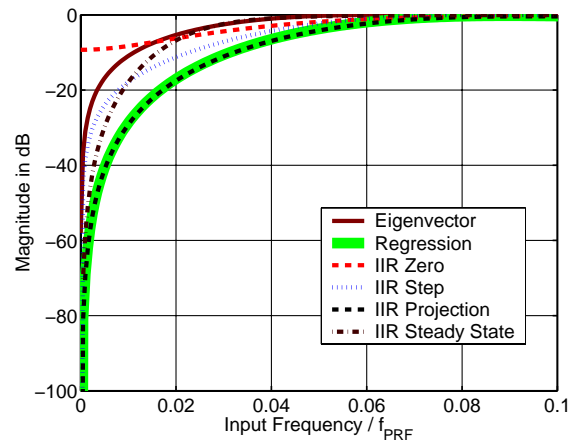


Fig.5: Frequency responses of high-pass filters. Only part of the pass-band is depicted. The maximum (aliasing) input frequency is equal to $0.5 \cdot f_{PRF}$.

experiment. A soft tissue-mimicking graphite-gelatin phantom (elastic modulus 18 kPa, [11]) was constructed with two cylindrical flow channels [12]. A blood-like scattering fluid — a 1% by mass suspension of cornstarch in water — flowed through the channels. The first channel (3 mm diameter) was connected to an infusion pump that generated steady Poiseuille flow with a maximum velocity of the parabolic flow-profile in the center of the channel of about 15 mm/s. The second channel (5 mm diameter) was connected to a peristaltic pump (5 pulses/s) to produce cyclic motion in the gelatin and modulate the steady flow in the first channel. We could not produce significant clutter from pulsatile gelatin motion using a single channel phantom without aliasing blood velocities. However, by separating the two effects into adjacent channels, it was possible to add clutter at approximately the same velocity as the blood flow, which provides the greatest challenge for clutter filters.

Data were acquired in M-mode from above the center of the 3 mm diameter channel using our laboratory scanner and a single-element spherically-focussed transducer (12.7 mm diameter, $f_0 = 15$ MHz, $f/3.5$). Fig. 6 depicts the color-coded velocities calculated by the 2-D autocorrelator which are overlaid on the regular brightness image. Without the pulsed pressure, the gelatin was motionless and flow in the 3 mm channel was steady over time and showed spatial velocities in the range (0...15) mm/s. With pulsed pressure, measured gelatin velocities ranged between ± 5 mm/s, and flow in the 3 mm channel was temporally modulated where the velocities ranged from (-1...30) mm/s. The softer flow channel strained more than the surrounding gelatin, so the large modulation in the channel is to be expected. Fig. 7 shows velocity maps corresponding to the color-flow image depicted in Fig. 6 after different clutter filters were applied. The zero-initialized

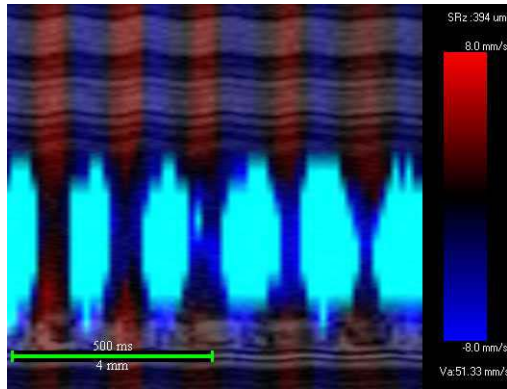


Fig.6: Color-flow M-mode image of pulsatile flow and pulsatile tissue motion. The horizontal time axis covers about 1 s. The ultrasound pulse duration of $0.5 \mu\text{s}$ matches the range gate length of approx. $400 \mu\text{m}$. The color flow velocity scale is adjusted to make the color-coded tissue motion clearly visible (the flow at peak pressure inside the channel is therefore out of range).

IIR filter is not able to suppress the gelatin motion (clutter) outside the channel. Step initialization suppresses clutter but also flow inside the channel. The regression filter significantly cancels clutter but also disturbs the flow profiles. Only the adaptive Eigenvector-based filter completely cancels all tissue motion and leaves the flow inside the channel almost unchanged.

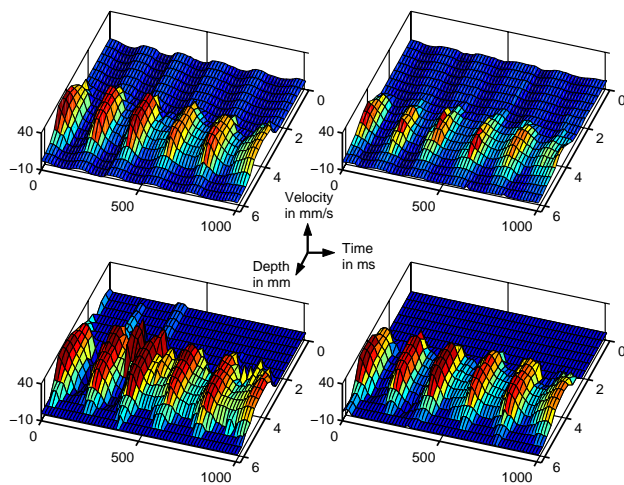


Fig.7: Different filters were applied to suppress tissue motion: zero initialized (top left) and step initialized (top right) second order IIR, first order regression (bottom left) and Eigenvector-based (bottom right) filters. The latter shows by far the best performance.

5 Conclusions

We showed that an extension of the well-known conventional autocorrelator can significantly improve the quality of flow estimation, especially for low velocities. Different clutter filters were also investigated and we were able to demonstrate that an adaptive Eigenvector-based approach provides excellent performance in discriminating between flow and clutter

even if the velocities are low and roughly the same in both parts. These are very promising results for the development of our combined flow-strain imaging, where strain is estimated from clutter to describe elastic properties and improve early detection of malignant tumors.

References:

- [1] I. Wu and M.A. Moses, Angiogenic molecules and mechanisms in breast cancer, *Curr Oncol Rep*, Vol. 2, No. 6, pp. 566-571, 2000.
- [2] T. Hasebe, K. Mukai, H. Tsuda, A. Ochiai, New prognostic histological parameter of invasive ductal carcinoma of the breast, *Path Int*, Vol 50, pp. 263-272, 2000.
- [3] R.A. Walker, The complexities of breast cancer desmoplasia, *Breast Cancer Res*, Vol. 3, No. 3, pp. 143-145, 2001.
- [4] Ch. Kargel, G. Plevnik, J.J. Mai, B. Trummer, C. Pellot-Barakat, M.F. Insana, Ultrasonic Strain-Flow Imaging, *Proc of Ultrasonics Internat 2001*, Technical Univ. of Delft, Netherlands.
- [5] C. Kasai, K. Namekawa, A. Koyano, R. Omoto, Real-Time Two-Dimensional Blood flow Imaging Using an Autocorrelation Technique, *IEEE Trans Son Ultrason*, Vol. SU-32, No. 3, May 1985.
- [6] D.S. Zrnik, Spectral Moment Estimators from Correlated Pulse Pairs, *IEEE Trans Aerospace Elect Sys*, Vol. AES 13, No. 4, pp. 344 - 354, 1977.
- [7] T. Loupas, R.B. Peterson, R. W. Gill, Experimental Evaluation of Velocity and Power Estimation for Ultrasound Blood flow Imaging, by Means of a Two-Dimensional Autocorrelation Approach, *IEEE Trans Ultrason Ferro Freq Contr*, Vol. 42, No. 4, 1995.
- [8] E. S. Chornoboy, Initialization for Improved IIR Filter Performance, *IEEE Trans Sig Proc*, Vol. 40, No. 3, 1992.
- [9] S. Bjaerum, H. Torp, Clutter Filter Design for Ultrasound Color flow Imaging, *IEEE Trans Ultrason Ferro Freq Contr*, Vol. 49, No. 2, 2002.
- [10] H. Torp, Clutter Rejection Filters in Color flow Imaging: A Theoretical Approach, *IEEE Trans Ultrason Ferro Freq Contr*, Vol. 44, No. 2, 1997.
- [11] Ch. Kargel, B. Trummer, G. Plevnik, C. Pellot-Barakat, J.J. Mai, M.F. Insana, Is Ultrasonic Imaging a sensitive Indicator of spatially varying elastic anisotropy? *Proc of IEEE Internat Ultrasonics Symposium 2001*, pp. 1659 - 1662, 2001.
- [12] J.J. Mai, M.F. Insana, Strain imaging of internal deformation, *Ultrasound Med Biol* (submitted March 2002).